journal of the mechanical behavior of biomedical materials 138 (2023) 105661

Contents lists available at ScienceDirect

Journal of the Mechanical Behavior of Biomedical Materials

journal homepage: www.elsevier.com/locate/jmbbm

Research paper

Computational modelling of the mechanical behaviour of protein-based hydrogels

Ángela Pérez-Benito [a], Carla Huerta-López [b], Jorge Alegre-Cebollada [b], José Manuel García-Aznar [a], Silvia Hervas-Raluy [a,*]

[a] Multiscale in Mechanical and Biological Engineering, Instituto de Investigacion en Ingenieria de Aragon(I3A), University of Zaragoza, Zaragoza, 50014, Spain
[b] Centro Nacional de Investigaciones Cardiovasculares (CNIC), Madrid, 28029, Spain

ARTICLE INFO

Keywords:
Biomaterials
Computational modelling
Protein-based hydrogels
Hyperelasticity
Viscoelasticity
Mechanical characterization

ABSTRACT

Protein-based hydrogels have been extensively studied in the field of biomaterials given their ability to mimic living tissues and their special resemblance to the extracellular matrix. Despite this, the methods used for the control of mechanical properties of hydrogels are very limited, focusing mainly on their elasticity, with an often unrealistic characterization of mechanical properties such as extensibility, stiffness and viscoelasticity. Being able to control these properties is essential for the development of new biomaterials, since it has been demonstrated that mechanical properties affect cell behaviour and biological processes. To better understand the mechanical behaviour of these biopolymers, a computational model is here developed to characterize the mechanical behaviour of two different protein-based hydrogels. Strain–stress tests and stress-relaxation tests are evaluated computationally and compared to the results obtained experimentally in a previous work. To achieve this goal the Finite Element Method is used, combining hyperelastic and viscoelastic models. Different hyperelastic constitutive models (Mooney–Rivlin, Neo-Hookean, first and third order Ogden, and Yeoh) are proposed to estimate the mechanical properties of the protein-based hydrogels by least-square fitting of the *in-vitro* uniaxial test results. Among these models, the first order Ogden model with a viscoelastic model defined in Prony parameters better reproduces the strain–stress response and the change of stiffness with strain observed in the *in-vitro* tests.

1. Introduction

Hydrogels are three-dimensional (3D) networks of physically or chemically cross-linked polymers with a high capacity to retain water or other biological fluids within them (Slaughter et al., 2009). These structures are highly biocompatible, as they provide an aqueous microenvironment very similar to the extracellular matrix (ECM) of living tissues (Slaughter et al., 2009; Peppas et al., 2000; Huerta-López and Alegre-Cebollada, 2021). Some of the characteristics that have drawn attention to these biomaterials are their ability to swell in aqueous media, their permeability, their optical properties, and their sensitivity to pH, temperature or other stimuli (Mahinroosta et al., 2018; You and Auguste, 2010). These unique properties make them suitable for a wide range of applications, such as their use in the development of biosensors, microfluidics, tissue engineering and controlled drug release (Mahinroosta et al., 2018).

Biological tissues have shown a high viscoelastic behaviour and exhibit stress relaxation in response to deformation, i.e., in response to a mechanical perturbation, they exhibit a time-dependent behaviour and a dissipation or loss of energy (Chaudhuri et al., 2020). It is well known in the field of mechanobiology that changes on the mechanical properties of the ECM can disrupt different cellular processes such as differentiation, fibrosis and malignancy (Yang et al., 2014; Stowers et al., 2019). So far, the view on this issue has been that substrate stiffness was the only parameter affecting cell behaviour (Smith et al., 2010). However, recent studies have shown that viscoelasticity also plays a major role in fundamental biological processes of living tissues, such as morphogenesis and motility (Mierke, 2022). In fact, it is now known that viscoelastic hydrogels can promote behaviours that are not observed with purely elastic hydrogels in both two- and three-dimensional culture microenvironments (Chaudhuri et al., 2020). A key objective in biomaterials research is to build hydrogels capable of replicating biological tissues, not only meeting a number of physical and biological requirements, but also being essential to match the mechanical and structural properties of the gel (tensile strength, stiffness, elasticity, etc.) to the specific tissue type (Buwalda et al., 2014), taking

* Corresponding author.
E-mail address: hervas@unizar.es (S. Hervas-Raluy).

https://doi.org/10.1016/j.jmbbm.2023.105661
Received 21 November 2022; Received in revised form 20 December 2022; Accepted 4 January 2023
Available online 6 January 2023

into account that these properties are often variable throughout their lifespan (Huerta-López and Alegre-Cebollada, 2021).

Protein hydrogels are a type of polymeric materials that use proteins as their building blocks (Mahinroosta et al., 2018). Proteins are essential molecules for the human body formed by effective macromolecular building blocks that offer unique functions based on their polypeptide structure, such as the support and functioning of cells, tissues and organisms, the transport of molecules and the catalysis of biochemical reactions, necessary to maintain cellular processes (Narupai et al., 2021). Consequently, one of the most remarkable behaviours found in protein hydrogels is the preservation of the properties inherent to their protein components (Gagner et al., 2014; Jabbari, 2019). However, it still remains an essential challenge to discern the connection between the mechanics of individual proteins and the macroscopic properties (Wu et al., 2018). These global mechanical properties of hydrogels are given by both properties of the individual filaments and the global architecture that may determine the cell behaviour inside these networks (Valero et al., 2018; Doyle et al., 2015).

Titin is a natural elastomeric protein and the largest protein encoded by the human genome. It is one of the main responsible for generating the passive elasticity of striated muscle as one of the main filaments of the sarcomere (Saqlain et al., 2015; Rassier, 2017). This protein is able to span half the length of the sarcomere adjusting to the needs of the working muscle (Krüger and Linke, 2011). Two complementary mechanisms contribute to the mechanical behaviour of titin: the entropic extension of the unstructured regions and the dynamic unfolding/refolding of ig-like and fn-like domains (Alegre-Cebollada et al., 2014). Moreover, force anisotropy on protein domains is another fundamental aspect of the protein mechanics, since the direction of the force applied determines the mechanical resistance of a globular protein (Eckels et al., 2016; Brockwell et al., 2003), which affect the chemical and mechanical properties of the final macroscopic behaviour (Kim et al., 2021). All these characteristics make titin an ideal protein for designing and engineering hydrogels with tunable mechanical properties.

To better understand the mechanics of biopolymers, different mathematical models have been investigated and developed with the aim of mimicking their behaviour of both single fibres and the fibres as a network (Wu et al., 2018; Shmilovich and Popa, 2018). The biopolymer models extend polymer theory to biological macromolecules to create biopolymer network models (Valero et al., 2018; Palmer and Boyce, 2008). Following this line, Kim et al. (2009) studied the relative contributions of thermal fluctuations of actin cytoskeleton network and the stiffness of filaments and linking proteins using a Brownian dynamics model, investigating viscoelastic moduli of actin-like networks. Additionally, due to the polymeric nature of the hydrogels, the viscoelastic mathematical models have been the most suitable to describe this type of materials, since the stress response consists of a combination of elastic and viscous behaviour (Chaudhuri et al., 2020; Ruymbeke et al., 2002; Heck et al., 2020). Fukunaga et al. (2019) developed a fractional constitutive model for solving dynamic problems of gel-like materials. However, there are models that have already been validated and are widely used capable of reproducing the visco-hyperelastic behaviour. Some researchers used the Prony series as long-term memory (time weight function) to extend the hyperelastic models to the visco-hyperelastic models, for instance, Ravikumar et al. (2015) showed that the use of the Ogden model with a Prony series term is sufficient to predict the visco-hyperelastic behaviour of a ballistic gelatin and Ghorbanoghli and Narooei (2019) used an hyper-viscoelastic constitutive modelling based on Prony series for self-healing hydrogels. Javadi et al. (2021) also implemented a hyper-viscoelastic model to study the behaviour of double-network hydrogels using long-term memory theory. The main advantages of these models are based on their easy implementation and their application as a basis for developing more complex models to study, for example, the interaction of cells with these matrices.

The aim of this work is to evaluate the mechanical behaviour of titin protein-based hydrogels through the development of a computational model based on Finite Element (FE) analysis. In this way, the main mechanisms responsible for the mechanical properties of this type of hydrogels are identified and the mechanical implications of varying the pulling geometry of the hydrogel polymeric networks can be analysed.

2. Materials and methods

2.1. Experimental analysis

Two hydrogels were computationally characterized based on the work developed by Huerta-Lopez et al. (2022), which preserved the same physical and chemical parameters. The main objective of this work was to evaluate the change in mechanical properties by modifying only the crosslinker points, i.e. how differences in pulling geometry affect the secondary structure and stability of polyproteins. These hydrogels were designed with the well-characterized I91 domain of titin Saqlain et al. (2015). In one hydrogel, crosslinking occurs in the linkers between domains (L2). However, in the other one, crosslinking takes place at the domains themselves (L3) [Fig. 1.A].

In the strategy followed by Huerta-Lopez et al. (2022), crosslinking occurs through tyrosine residues present in the protein building blocks. L2 (I91-Y9P) hydrogels present a mutation in the position 9 of the I91 domain, where the original tyrosine has been mutated and replaced by a proline. The linker sequence of L2 (I91-Y9P) polyproteins coincides with that of their L3 (I91) counterparts with the sole difference of replacing one of the serine residues by a tyrosine. Hence, when strain is applied uniaxially to L2 (I91-Y9P) hydrogels, the I91-Y9P building blocks, which are crosslinked only through the linkers between domains, only experience N-terminal to C-terminal force, differently from L3 building blocks that are subject to an additional pulling direction through crosslinked Tyr9 residues [Fig. 1A]. The nomenclature of the L2 and L3 refers to the length of linkers between domains and the number of pulling points involved in the propagation of force through the polyproteins when these are subjected to uniaxial traction. In both constructs, linkers are 11 amino acids long, which the authors classify as long or L. The change in nanoscale geometries is enough to alter the mechanical response of the resulting crosslinked hydrogel with only minor modifications of structural and biochemical properties (Huerta-Lopez et al., 2022).

In order to characterize the mechanical behaviour of these materials, uniaxial and stress-relaxation *in-vitro* tests were performed in 50 mM sodium phosphate pH 7.5, 150 mM NaCl buffer at room temperature. Tensile tester was designed including the basic elements that assemble a universal tester, which we adapted to the force range the specimens needed. The tensile tester includes a force sensor and a linear actuator connected to the specimen, which is gripped using tweezers. The electronics of both devices feed into a computer using a data acquisition card, which allows for reciprocal communication. In this setup, cylinder shaped hydrogels (0.506 mm diameter and 10 mm long) were fixed at both ends by tweezers attached to both the load cell and the linear actuator. Further experimental details can be found in Ref. Huerta-Lopez et al. (2022). Uniaxial tests were performed at different defined strain values, from 20% to 100%, to obtain the forward and backward stress–strain plots. The strain rates in these assays was 5 mm/s. The evolution of the Young modulus over the loading cycle was determined. Specifically, the secant modulus (E^{sec}) was calculated as the slope of the straight line joining the initial stress–strain point with each point on the stress–strain plot.Stress-relaxation tests were performed under constant strain while the load is recorded as a function of time. Relaxation measurements at strains that produced 20 kPa or 50 kPa initial stress at a strain rate of 5 mm/s were conducted. Thus, different strains were applied to each hydrogel type, so the same stress was reached depending on their apparent elastic moduli. Deformation values were fixed for 30 min.

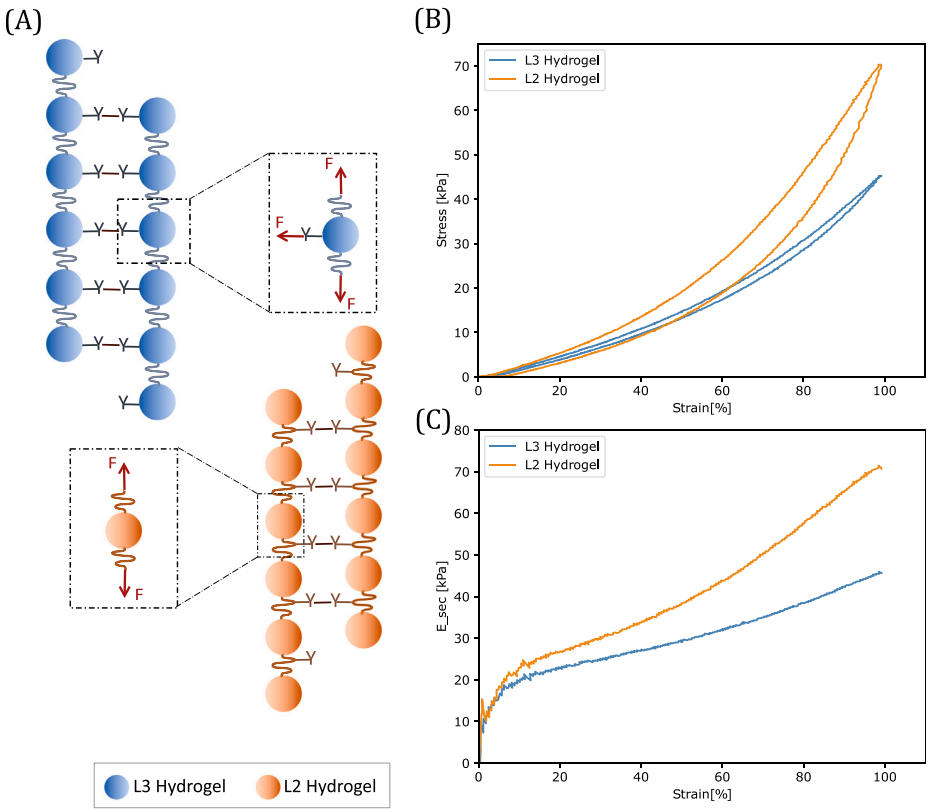

Fig. 1. (A) Crosslinking in L3 hydrogel in blue and L2 hydrogel in orange and the direction of the forces in an uniaxial essay. (B) Stress–strain plot in uniaxial essay. (C) Elastic modulus (Huerta-Lopez et al., 2022).

Both hydrogels perform in the range of large deformations and present a time-dependent response. It can be noted that a change in the nanoscale the pulling geometry applied to protein building blocks, effectively modulates hydrogel viscoelasticity. Specifically, L2 hydrogels are stiffer and more dissipative than L3 [Fig. 1.B, C] (Huerta-Lopez et al., 2022).

2.2. FE-based computational model

Due to the given characteristics presented by the hydrogels described in Section 2.1, a combination of hyperelastic and viscoelastic models is implemented to simulate the uniaxial and stress-relaxation tests, by means of a FE analysis.

2.2.1. Hyperelastic contribution

Different hyperelastic models are tested in order to find the model that better explains the crosslinked hydrogel behaviour observed *in vitro*. The mechanical behaviour of hyperelastic materials is given by the relation between strain energy density and the three invariants of the strain tensor ($\bar{I}_1$, $\bar{I}_2$ and $\bar{I}_3$), or the three principal expansion ratio ($\bar{\lambda}_1$, $\bar{\lambda}_2$ and $\bar{\lambda}_3$) (Ghoreishy, 2012). Among the existing hyperelastic models, five of them are compared: the Mooney–Rivlin model, the Ogden model (first and third order), the Neo-Hookean model and the Yeoh model.

The form of the Mooney–Rivlin strain energy potential (Shahzad et al., 2015) is defined by a linear combination of the first two invariants ($\bar{I}_1$, $\bar{I}_2$) of the left Cauchy–Green deformation tensor, being as follows:

$$\psi = C_{10}(\bar{I}_1 - 3) + C_{01}(\bar{I}_2 - 3) + \frac{1}{D_1}(J_{el} - 1)^2 \tag{1}$$

where C_{10} and C_{01} are the material constants that control the shear behaviour and can be determined from uniaxial, biaxial and planar tests; D_1 is a material constant that control bulk compressibility, being zero when the material is fully incompressible; and J_{el} is the elastic volume ratio (Shahzad et al., 2015).

Secondly, the Neo-Hookean model (García Ruíz and González, 2006) is a particular case of Mooney–Rivlin model where $C_{01} = 0$. This model is one of the most simplest hyperelastic models, since initially it follows a linear response between strain and stress applied until it reaches certain point when the stress–strain plot changes to nonlinear (Shahzad et al., 2015; Kim et al., 2012). The strain density function is defined as follows:

$$\psi = C_{10}(\bar{I}_1 - 3) + \frac{1}{D_1}(J_{el} - 1)^2 \tag{2}$$

Following, the Ogden model has been frequently used in for the analysis of polymers and rubber-like materials. It can be described in terms of principal stretch ratios ($\bar{\lambda}_1$, $\bar{\lambda}_2$, $\bar{\lambda}_3$) instead of invariants (Kim et al., 2012; Shahzad et al., 2015), defined as:

$$\psi = \sum_{i=1}^{n} \frac{2\mu_i}{\alpha_i^2}(\bar{\lambda}_1^{\alpha_i} + \bar{\lambda}_2^{\alpha_i} + \bar{\lambda}_3^{\alpha_i} - 3) + \sum_{i=1}^{n} \frac{1}{D_i}(J_{el} - 1)^{2i} \tag{3}$$

where $2\mu_i$ and α_i are material constants and n is the order of the model.

Lastly, the Yeoh model is a third order reduced polynomial model and is based on the first strain invariant (Kim et al., 2012; Shahzad et al., 2015), as follows:

$$\psi = \sum_{i=1}^{3} C_{i0}(\bar{I}_1 - 3)^i + \sum_{i=1}^{3} \frac{1}{D_i}(J_{el} - 1)^{2i} \tag{4}$$

2.2.2. Viscoelastic contribution

The viscoelastic time-domain material model describes the velocity-dependent isotropic material behaviour for materials in which dissipative losses are mainly caused by viscous (internal damping) effects. It is assumed that the deviatoric shear and volumetric behaviours are independent in multi-axial stress states (Smith, 2014).

In this work, the generalized Maxwell model is used as a combination of several Maxwell elements assembled in parallel to describe the viscoelastic contribution (Romero et al., 2020). Maxwell model can be defined by a Prony series expansion of the dimensionless relaxation modulus as it is shown in Eq. (5):

$$g_R = 1 - \sum_{i=1}^{N} g_i(1 - e^{\frac{-t}{\tau_i}}) \tag{5}$$

where N is the number of Prony series, g_i is the ith value of the ratio of the shear relaxation modulus of the material which can be obtained from the form: $g_i = G_i/G_0$; where G_i is the value of the shear modulus of the ith spring in the ith Maxwell element and G_0 is the value of the instantaneous shear modulus of rigidity of the generalized Maxwell model, τ_i is the value of the relaxation time of the ith Maxwell element within the model. This value is defined as the ratio of the viscosity of the damper to the modulus of elasticity of the spring of the ith Maxwell element: $\tau_i = \eta_i/E_i$ (Smith, 2014).

A similar Prony series expansion is used for the volumetric response

$$p = -K_0\left(\varepsilon^{vol} - \sum_{i=1}^{N} \varepsilon_i^{vol}\right) \tag{6}$$

where ε_i^{vol} is defined as:

$$\varepsilon_i^{vol} = \frac{k_i}{\tau_i}\int_0^t e^{\frac{-s}{\tau_i}}\varepsilon^{vol}(t-s)ds \tag{7}$$

and k_i is the ith value of the ratio of the volumetric modulus of relaxation of the material which can be obtained from the form: $k_i = K_i/K_0$; where K_i is the value of the volumetric modulus of the ith spring in the ith Maxwell element and K_0 is the value of the instantaneous volumetric modulus of rigidity of the generalized Maxwell model (Smith, 2014).

2.2.3. Model fitting

In order to characterize the mechanical response observed *in-vitro*, an inverse problem of curve fitting is solved using an iterative approach based on the least squares method. This method minimizes a cost function (CF) defined by a standard sum of squared differences in stress (Sainz-DeMena et al., 2022), as it is shown in Eq. (8), minimizing the relative error.

$$CF = \sum_{i=1}^{n}\left(1 - \frac{\sigma_i^{comp}}{\sigma_i^{test}}\right)^2 \tag{8}$$

where n is the number of test data points, σ_i^{test} is a stress value from the test data, and σ_i^{comp} is the nominal stress obtained by the computational hyperelastic models.

Moreover, in order to obtain a better calibration, the Drucker stability is analysed. Thus, a material cannot satisfy this criteria when a load applied to a point leads to arbitrary deformations. The condition that an incompressible material must meet for this criterion to be fulfilled is the following (Ahearne et al., 2005)

$$d\sigma : d\varepsilon > 0 \tag{9}$$

where $d\varepsilon$ is the change in the logarithmic strain and $d\sigma$ is the change in stress, using $d\sigma = \boldsymbol{D} : d\varepsilon$, being $\boldsymbol{D}$ the tangent material stiffness. So the tangent material stiffness is required to be positive for material stability. The value of the constants C_{ij} for the polynomial models and μ and α for the Ogden form [Eq. (3)] must be defined in order to meet this condition. When some of these coefficients are strongly negative, instability at higher strains is likely to occur.

The least-square method presented in Eq. (8) is also used to fit the Prony parameters of the viscoelastic behaviour: g, k and τ. An error tolerance of 0.01 is defined as the allowable average root-mean-square error of data points in the least-squares fit. The least square fit is performed until convergence is achieved for the lowest number of series of Prony with respect to error tolerance.

2.3. Numerical implementation

The different experimental tests are simulated via the FE Method using the commercial software ABAQUS (Dassault Systemes, Vlizy-Villacoublay, France). The geometry used consists of a cylinder of 0.506 mm diameter and 10 mm length and it is discretized using a quadrilateral, axisymmetric linear element mesh, obtaining a total of 204 nodes and 150 elements. Fig. 2 represents the input FE model in ABAQUS, considering axisymmetry and symmetry in the transversal direction of the bar (restricted displacements in the longitudinal direction at the base of the bar). Loads are applied at the opposite end of the bar. The ABAQUS material calibration module is used to find the parameters that best fit, both for the hyperelastic and viscoelastic parameters [Eq. (8)] (Farid, 2020; Smith, 2014).

Afterwards, to compare experimental and computational tests, the relative error at different strain points is calculated, as shown in Eq. (10).

$$RE = \left|\frac{\epsilon_e - \epsilon_c}{\epsilon_e}\right| \tag{10}$$

where RE is the relative error, ϵ_e is the experimental value and ϵ_c is the computational value.

3. Results

In this section, we present the numerical results obtained from simulation in comparison with experimental measurements from previous work (Huerta-Lopez et al., 2022). First, the model fitting of the different hyperelastic constitutive models (Mooney–Rivlin, Neo-Hookean, first and third order Ogden, and Yeoh) is shown for the L2 and L3 hydrogels, giving a comparison between the computational models exposed and the *in-vitro* tests. Secondly, the Prony parameters and number of series needed to define the viscoelastic behaviour are obtained. Next, uniaxial and stress-relaxation tests are numerically simulated for the L2 hydrogel, implementing a combined first order Ogden model with the viscoelastic model, and the results are compared with the *in-vitro* tests. The change in stiffness with strain is also analysed for *in-silico* and *in-vitro* tests. Finally, the same procedure is followed with L3 hydrogel.

The comparison between the experimental and the computational results obtained with the different hyperelastic computational models presented in Section 2.2.1 is represented in Fig. 3. The fitting errors obtained with Eq. (8) for each hydrogel and every hyperelastic model are presented in Table 1. The Neo-Hookean plot presents the highest error for both hydrogels, reaching a fitting error of almost 80% for L2 hydrogel. In fact, Fig. 3 shows that this model cannot capture the upturn of stress–strain plot, describing a quasi-linear behaviour and obtaining stresses much lower than the desired for high strains. The Mooney–Rivlin, Yeoh and third order Ogden model do better capture the behaviour, presenting the third order Ogden model the best fitting for both hydrogels. However, these three models present strongly negative constant materials [Supplementary Tables A.4, A.5 and A.7]. Therefore, these models are unstable in the range of deformation analysed. To avoid instabilities and to make a better quality adjustment, we selected the first Ogden model, that also gives a low fitting error (1.84% for L3 hydrogel and 6.67% for L2 hydrogel) and the fitting of the stress–strain plot is highly accurate for both hydrogels, being stable in all the range of deformation. Table 2 shows the coefficients obtained in the fitting process.

As for the hyperelastic behaviour, the viscoelastic behaviour is adjusted. Two series of Prony are enough to describe this behaviour of L3 and L2 hydrogels [Table 3].

The L3 hydrogel experimentally presents a smaller variation in stiffness with fibre stretching than the L2 hydrogel, and also dissipates less energy. The different stress–strain plots performed at final strains 20%, 40%, 60%, 80% and 100% for the experimental and computational L3 gels are shown in Fig. 4A. As the different cycle plots are superposed, so

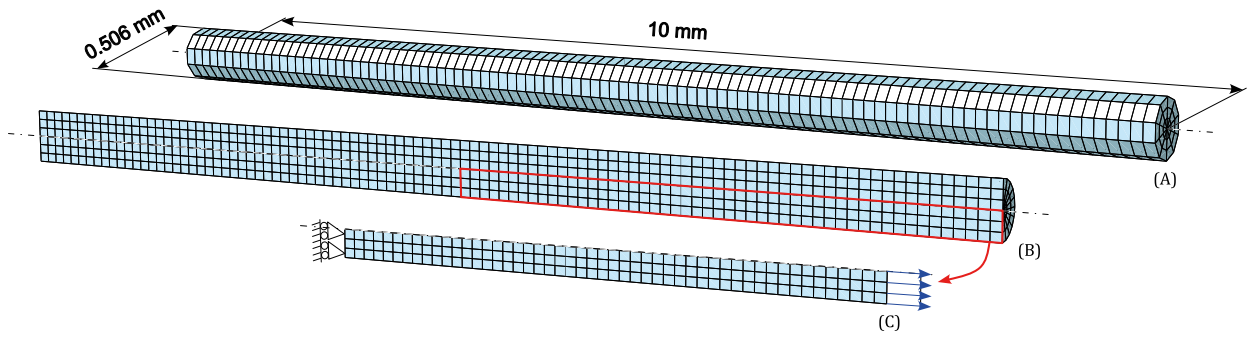

Fig. 2. FE-based model to simulate experimental conditions. (A) Measurements of the specimen; (B) Cutaway view of the mesh; (C) Axisymmetric model to simulate using ABAQUS.

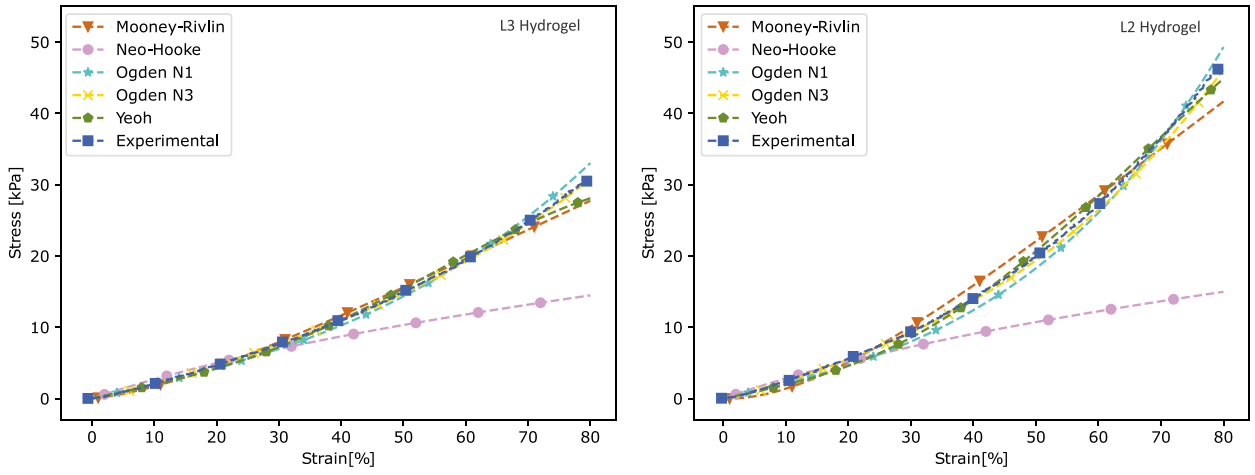

Fig. 3. Comparison between the experimental uniaxial test and the uniaxial tests performed with the hyperelastic computational models presented at a strain of 80%, for L3 hydrogel on the left and L2 on the right.

Table 1
Fitting errors obtained using the cost function described in Eq. (8) for the different hyperelastic models.

Fitting error [%]		
Hyperelastic model	L3 hydrogel	L2 hydrogel
Mooney–Rivlin	0.9497	5.246
Ogden N1	1.836	6.672
Ogden N3	0.1808	1.103
Neo-Hookean	30.95	78.36
Yeoh	1.463	5.232

Table 2
Coefficients corresponding to the Ogden's N = 1 material model Eq. (3).

	μ_1	α_1	D_1
L3 hydrogel	6.74	5.43	0
L2 hydrogel	6.82	6.37	0

Table 3
Coefficients corresponding to the Prony series Eq. (5).

	g_1	k_1	τ_1	g_2	k_2	τ_2
L3 hydrogel	0.17	0	4.44	0.13	0	188.38
L2 hydrogel	0.22	0	3.28	0.15	0	131.56

they are offset in Fig. 4B, C and D for clarity. In Fig. 4B, the experimental and computational stress–strain cycles are included and in Fig. 4C and D the loadings and unloadings plots of the cycle are represented respectively. It can be seen in Fig. 4C that the computational loading plots fit to the experimental one, obtaining errors under 25% for almost the entire cycles. The computational results present lower stresses before they reach 40% deformation. It can be noted that the maximum errors occurs at the beginning of the cycles. In contrast to the observed experimental hydrogel behaviour when imposing deformation back to zero [Fig. 4D] -the stresses on the unloading plot are lower than on the loading plot, reaching the maximum difference at the halfway point-, the computational plot reaches the maximum difference between loading and unloading stresses at 0% strain, which means that if it is not given time to recover, the hydrogel is held in negative stresses. Moreover, this fact makes a significant difference in how the energy is dissipated. In general, the viscoelastic response of computational hydrogels is much lower than the experimental ones.

The experimental and computational elastic modulus of L3 hydrogel are compared in Fig. 5A. Only the elastic modulus obtained in the stress–strain experiment at 100% final strain is plotted, since a similar behaviour is observed in the rest of the conditions. As this material follows a non-linear behaviour, this modulus is not constant and grows with increasing deformation. It can be seen that the computational plot shows a drastic increase at the beginning of the cycle, and once this point is reached, an exponential growth follows. In contrast, the experimental plot has a slightly more gradual start and then grows smoother. As expected, the errors are maximum at lower deformations, being less of 25% at the rest of the cycle.

To determine the relaxation response of L3 hydrogel, we replicate the test at a initial stress value of 50 kPa and 20 kPa [Fig. 5B]. For both hydrogels, at a fixed strain value, the stress shows a faster decrease in the initial times, until it reaches a plateau value. The higher the initial stress value is, the slower it reaches this plateau value. At a initial stress value of 20 kPa the computational plot presents lower stresses, therefore the plateau value is reached later on. Then, both plots present a similar slope until the end of the test, obtaining an error of 15% (19 kPa

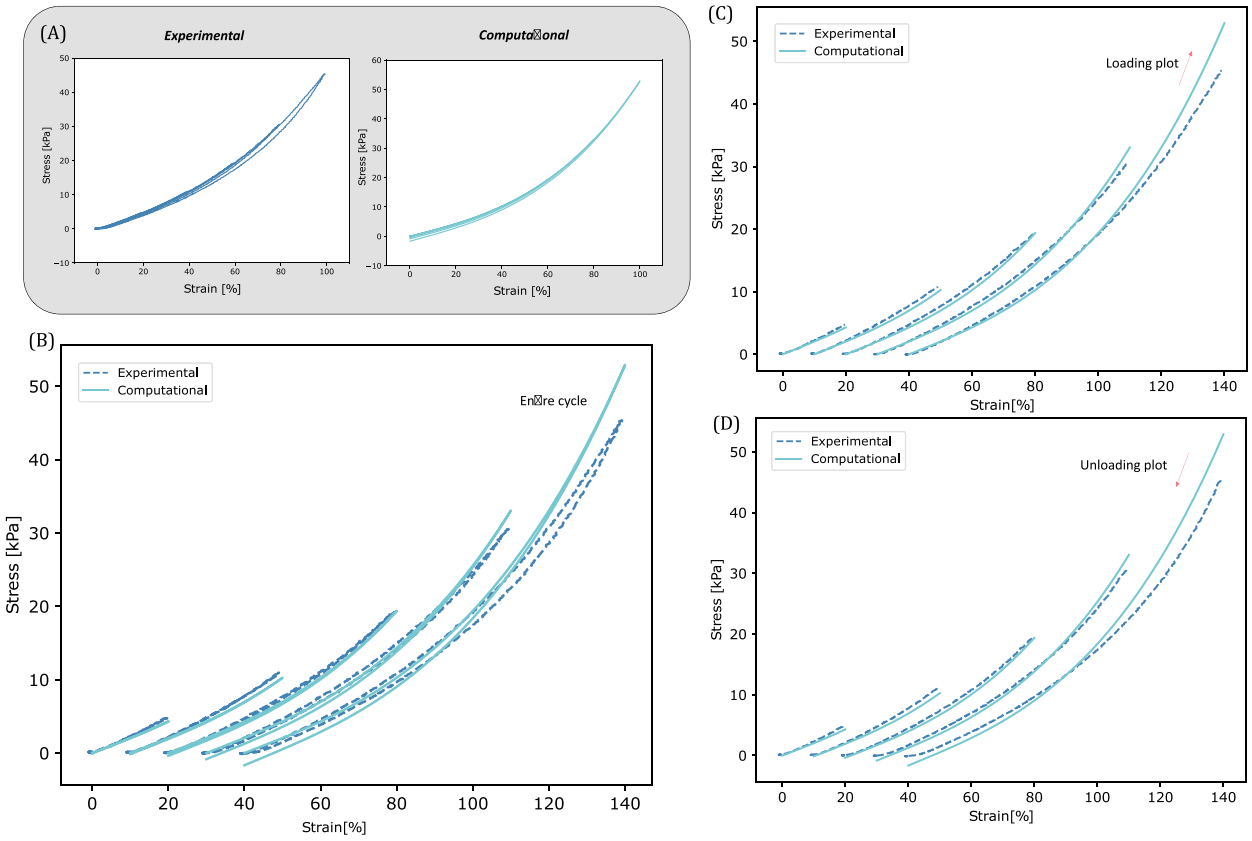

Fig. 4. (A) L3 Hydrogel uniaxial test performed at strains 20%, 40%, 60%, 80% and 100% for the experimental (left) and computational (right) gels performed with the first order Ogden model. For clarity, stress–strain plots are offset relative to one another: (B) Entire cycle; (C) Loading plots; (D) Unloading plots.

for the experimental, and 14 kPa for the computational). However, at the initial stress value of 50 kPa, the computational plot presents higher stresses along time than the experimental one, even though the computational reaches a plateau value of 36 kPa, the experimental one seems to gradually lowers. Nevertheless the error is almost negligible between this plots until 400 s.

The L2 hydrogel has a stiffer response with fibre stretching than L3 hydrogel and its viscoelastic response is higher, dissipating more energy the greater the fibre stretch. The different stress–strain plots performed at final strains 20%, 40%, 60%, 80% and 100% for the experimental and computational L2 gels are shown in Fig. 6A. As happens with L3 hydrogel, the different cycle plots are superposed, so they are offset in Fig. 6B, C and D, so the stress–strain plots for the different strain cycles can be seen more clearly. In Fig. 6B, the experimental and computational stress–strain cycles are represented and in Fig. 6C and D the loading and unloading plots of the cycle are represented respectively. The model simulates the behaviour of the experimental loading response accurately, obtaining errors lower than 25% for almost the entire cycle and for the different plots. The computational tests experiment lower stresses until they reach 60% of strain, which then exceed the experimental plots as we can see in Fig. 6C. More differences are found at the unloading plots [Fig. 6D]. The computational unloading plots present higher stress difference than the loading plots when the deformation approaches zero. However, in the experimental plots the difference between stresses in the loading and unloading plots were higher at the middle of the trajectory, this difference being zero at the maximum and minimum strain. This translates into a higher difference in the amount of energy dissipated on the entire cycle, as the experimental hydrogels have a higher viscoelastic contribution than the computational ones.

The experimental and computational elastic modulus of L2 hydrogel are compared in Fig. 7A. Only the elastic modulus in the test to 100% is plotted, since a similar behaviour is observed in the rest of the plots, as in L3 hydrogel. Since this material follows a non-linear behaviour, this modulus is not constant but grows as the deformation increases. The experimental plot grows faster until it reaches a strain of 15%, when it starts to grow more gradually. In contrast, the computational plot shows a drastic increase when the test starts, and describes a exponential growth starting with a elastic modulus value of 20 kPa. Nevertheless, both experimental a computational plots experiment a similar behaviour and the error obtained are lower than 25%.

The stress-relaxation test at a initial stress values of 50 kPa and 20 kPa for L2 hydrogel is replicated in Fig. 7B. For both hydrogels, at a fixed strain value, the stress shows a faster decrease in the initial times, until it reaches a plateau value. At a initial stress value of 20 kPa the computational plot presents lower stresses than the experimental one. However, the difference between both plots is almost negligible, being 10% the maximum error obtained. The computational plot reaches a value of 13.24 kPa stress after 300 s and maintains it until the end of the experiment, unlike the experimental plot, that, after 250 s, decreases very slowly, reaching 13 kPa at the end of the test.

At the initial stress value of 50 kPa, the computational plot presents higher stress values than the experimental one. Even though the computational stress values reach a plateau value of 31.7 kPa, the experimental values seems to gradually lowers with time, increasing the error. However the error is almost negligible between these plots until the time of 300 s, when both plots separate and the difference between them increases. Nevertheless, the error is always lower than 10%, reaching this value at the end of the test.

4. Conclusions and discussion

The mechanical response of two different hydrogels, based on protein titin (L3 and L2) with the same physical and chemical parameters,

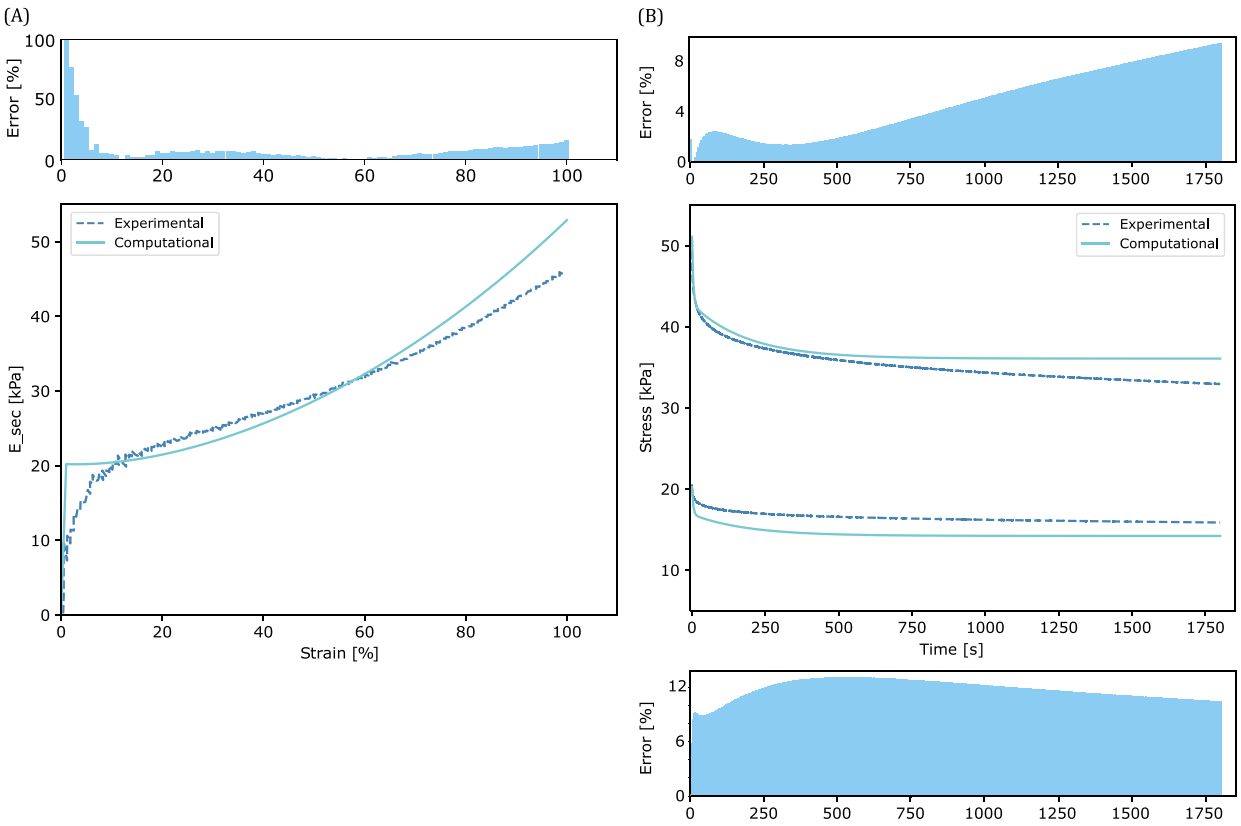

Fig. 5. (A) L3 Hydrogel secant elastic modulus at a 100% strain for the experimental and computational first order Ogden model gels (below) and the relative error between them (above). (B) L3 Hydrogel stress-relaxation test, at a initial stress value of 50 kPa and 20 kPa, for the experimental and computational gels, and the error obtained between them: above for the initial stress of 50 kPa and below for the initial stress of 20 kPa.

but different crosslink points, is simulated. For this aim, uniaxial and stress-relaxation *in-vitro* tests are modelled by means of FE Analysis. Both hydrogels present a visco-hyperelastic behaviour, but the difference in their crosslink points impacts significantly in their mechanical response, as it has been shown in previous studies (Huerta-Lopez et al., 2022). The L2 hydrogel presents its crosslinking points at the inter-domain links while the L3 hydrogel presents them at the domains themselves. Mechanically, this results in a stiffening of the L2 hydrogel and a higher dissipative response (Huerta-Lopez et al., 2022).

The main objective of this work is to *in-silico* mimic the mechanical behaviour of this two hydrogels tested *in-vitro*. In order to achieve that, a calibration method is performed to find the constitutive law that better reproduce the material mechanical behaviour, combining a hyperelastic and a viscoelastic model.

An iterative approach based on the least squares method is used to calibrate the different models presented (Mooney–Rivlin, Neo-Hookean, first and third order Ogden, and Yeoh models and the viscoelastic model), minimizing the relative stress error. The Neo-Hookean model gives the worst fitting for both hydrogels, not being able to accurately predict phenomena at large strains, in agreement with literature (Kim et al., 2012). The Mooney–Rivlin, third order Ogden and Yeoh models show a better fitting, but present instabilities at large strains. The first order Ogden is able to mimic the mechanical response of both hydrogels observed *in vitro*. To replicate the viscoelastic response of the L3 and L2 hydrogels two series of Prony are needed. Using the first order Ogden model and the Prony parameters to describe the material behaviour, it is possible to modulate the stress–strain response of these two computational hydrogels with different mechanical characteristics. By setting higher values to the material constants of the Ogden model in L2 hydrogel, a increase in its stiffness is achieved in contrast to the L3 hydrogel, whose mechanical response is softer. For the viscoelastic behaviour, we get a higher energy dissipation for the L2 hydrogel than for the L3 hydrogel, matching this with the experimental test results.

An accurate fitting of the hyperelastic behaviour on the loading plot of the uniaxial tests is achieved, getting more stress difference between computational and experimental plot at higher strains for both hydrogels. This might be due to the fact that the calibration was done with the test up to 80% strain, so at higher ranges of deformation the fitting is not sufficient accurate. Nevertheless, the smallest fitting errors for all strain–stress curves are obtained calibrating in this manner. In the secant elastic modulus plot the same trend can be appreciated, as the stress–strain data is used to calculate the stiffness. The unloading plot of computational uniaxial tests does accurately predict the response of experimental materials. For L3 and L2 computational hydrogels, at the end of the uniaxial test, residual stresses are stored while the experimental ones are not. However, the computational stress-relaxation tests reproduce well the behaviour of the experimental ones for both hydrogels and at different stress start points. This significant difference is a result of the fact that stress-relaxation test is used to calibrate the viscoelastic behaviour. In future work, more experimental test data or other calibration methods will be needed in order to get a more accurate calibration to capture the viscous behaviour of these materials in an uniaxial test.

ECM mechanics plays an important role in physiological and pathological cellular processes. Therefore, the development of hydrogels capable of mimicking the ECM and reproducing a wide range of mechanical properties is essential in understanding how mechanical factors of the substrate affect cells and diverse cellular processes (Cacopardo et al., 2022). Furthermore, these gels can be used for generating physiologically relevant *in vitro* models and to improve the performance of tissue substitutes for regenerative medicine applications (Cacopardo et al., 2022). It has been proven that stiffness is a key parameter involved in processes such as spreading, migration, differentiation and tumorigenesis (Wozniak and Chen, 2009; Levental et al., 2007). Even though, given the complex nature of ECM, it should be expected

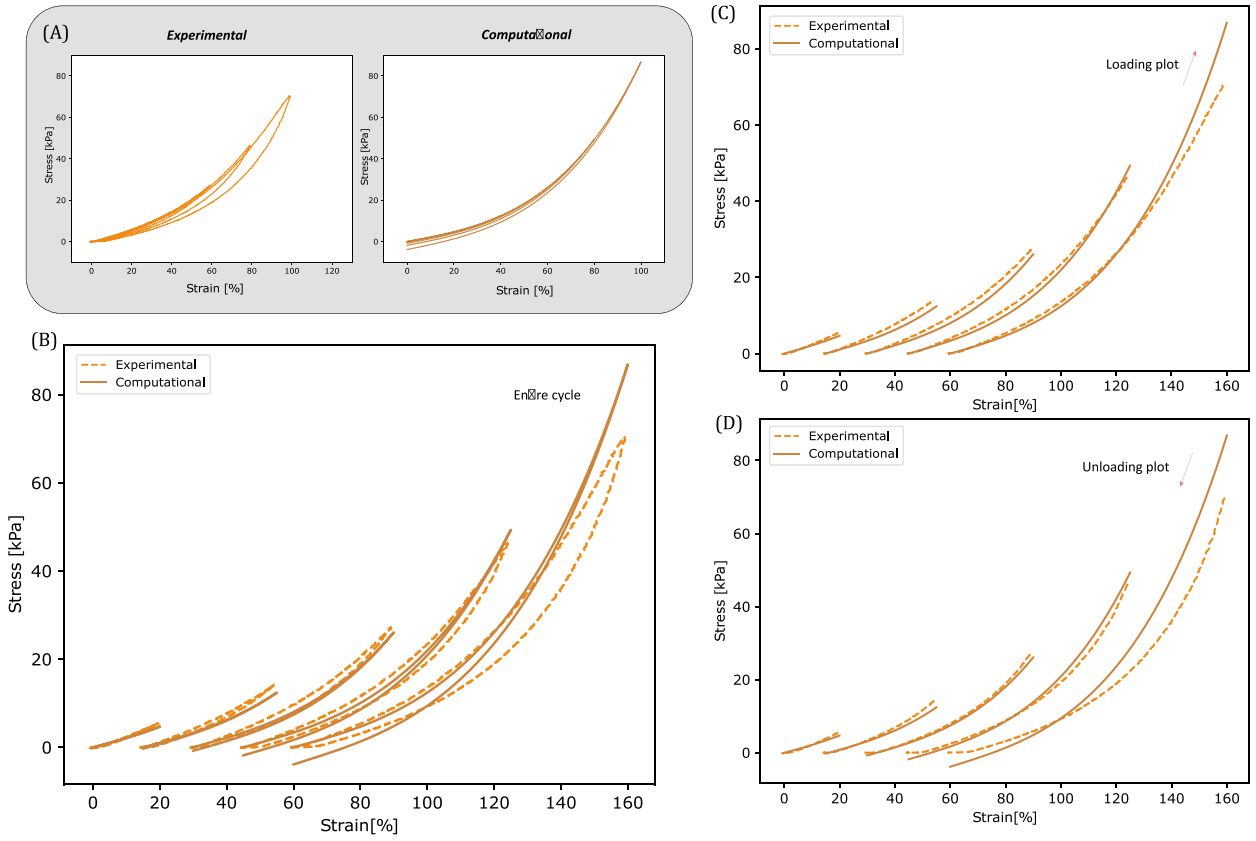

Fig. 6. (A) L2 Hydrogel uniaxial test performed at strains 20%, 40%, 60%, 80% and 100% for the experimental (left) and computational (right) gels performed with the first order Ogden model. For clarity, stress–strain plots are offset relative to one another: (B) Entire cycle; (C) loading plots; (D) unloading plots.

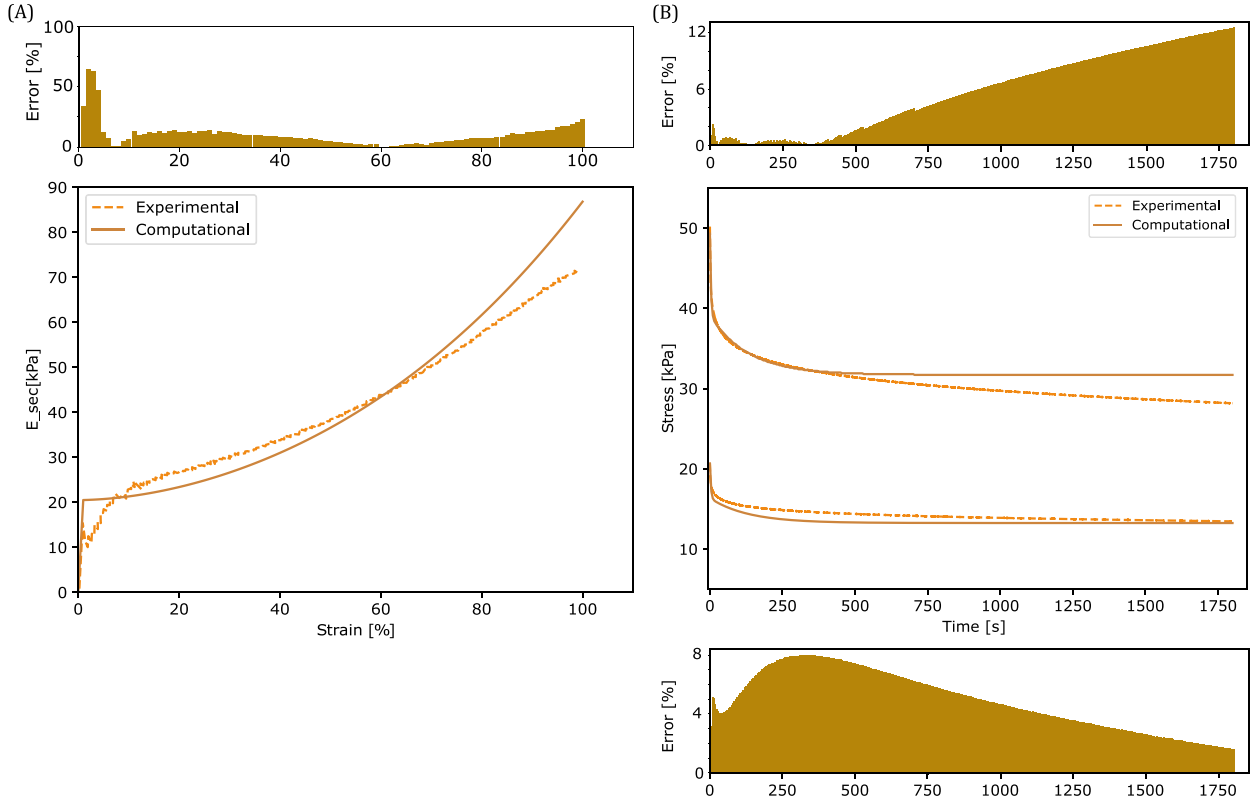

Fig. 7. (A) L2 Hydrogel secant elastic modulus at a 100% strain for the experimental and computational first order Ogden model gels (below) and the relative error between them (above). (B) L2 Hydrogel stress-relaxation test, at a initial stress value of 50 kPa and 20 kPa, for the experimental and computational gels, and the error obtained between them: above for the initial stress of 50 kPa and below for the initial stress of 20 kPa.

that time-dependent mechanical responses affect cell–ECM interactions and mechanotransduction (Cacopardo et al., 2022). The protein-based hydrogels described in this work present different stiffness and energy dissipation characteristics, whilst trying to avoid modification of non-mechanical parameters, which can help to better analyse the effect of substrate viscoelasticity on cell biology and how mechanical forces address shape cell and tissue function (Huerta-Lopez et al., 2022). The development of *in-silico* models capable of simulating this kind of materials can give a wide overview in the study of the interaction between cell and ECM. With computational modelling, the number of *in-vitro* experiments could be reduced, with the cost reduction in both time and financial terms that this entails. The model developed in this work can be further explored to predict the behaviour of cells in different mechanical microenvironments and how this may also affect mechanotransduction. Such assays may be relevant in different areas of study where hydrogels are currently proving to have many advantages, from which we have highlighted tissue and biomedical engineering, drug delivery and mechanobiology. Therefore, the described model could be applied to other hydrogels in an ample range of mechanical properties to cover the scope of tests required in the areas of study.

CRediT authorship contribution statement

Ángela Pérez-Benito: Writing – original draft, Visualization, Validation, Software, Methodology, Investigation, Data curation. **Carla Huerta-López:** Writing – review & editing, Methodology, Investigation, Formal analysis, Data curation. **Jorge Alegre-Cebollada:** Writing – review & editing, Resources, Funding acquisition, Conceptualization. **José Manuel García-Aznar:** Writing – review & editing, Supervision, Project administration, Methodology, Funding acquisition, Formal analysis, Conceptualization. **Silvia Hervas-Raluy:** Writing – review & editing, Supervision, Methodology, Formal analysis.

Declaration of competing interest

The authors declare that they have no known competing financial interests or personal relationships that could have appeared to influence the work reported in this paper.

Data availability

Data will be made available on request.

Acknowledgements

APB was supported by MCIN/AEI/10.13039/501100011033/ and by European Union NextGeneration EU/PRT through the project PLEC2021-007709 (ProCanAid) the Aragon Institute for Engineering Research (I3A). SHR gratefully acknowledges the support of the Government of Aragon (Grant no 2019-23). The work of JMGA was supported by the European Research Council (ERC) under the European Union's Horizon 2020 research and innovation programme (Advance grant agreement ICoMICS No 101018587) and the Spanish Ministry of Economy and Competitiveness, Spain Grant No PID2021-122409OB-C21/AEI/10.13039/501100011033/ FEDER, UE. JAC acknowledges funding from the Ministerio de Ciencia e Innovación (MCIN), Spain through grant BIO2017-83640-P (AEI/FEDER, UE). CNIC is supported by the Instituto de Salud Carlos III (ISCIII), MCIN, Spain and the Pro CNIC Foundation, and is a Severo Ochoa Center of Excellence, Spain (grant CEX2020-001041-S funded by MCIN/AEI/10.13039/501100011033). CHL was the recipient of an FPI predoctoral fellowship, Spain (BES-2015-073191).

Appendix A. Supplementary data

Supplementary material related to this article can be found online at https://doi.org/10.1016/j.jmbbm.2023.105661.

References

Ahearne, M., Yang, Y., Haj, A.J.E., Then, K.Y., Liu, K.K., 2005. Characterizing the viscoelastic properties of thin hydrogel-based constructs for tissue engineering applications. J. R. Soc. Interface 2, 455–463. http://dx.doi.org/10.1098/rsif.2005.0065.

Alegre-Cebollada, J., Kosuri, P., Giganti, D., Eckels, E., Rivas-Pardo, J.A., Hamdani, N., Warren, C.M., Solaro, R.J., Linke, W.A., Fernández, J.M., 2014. S-glutathionylation of cryptic cysteines enhances titin elasticity by blocking protein folding. Cell 156, 1235–1246. http://dx.doi.org/10.1016/J.CELL.2014.01.056.

Brockwell, D.J., Paci, E., Zinober, R.C., Beddard, G.S., Olmsted, P.D., Smith, D.A., Perham, R.N., Radford, S.E., 2003. Pulling geometry defines the mechanical resistance of a beta-sheet protein. Nat. Struct. Mol. Biol. 10 (9), 731–737. http://dx.doi.org/10.1038/nsb968, 10 (2003).

Buwalda, S.J., Boere, K.W., Dijkstra, P.J., Feijen, J., Vermonden, T., Hennink, W.E., 2014. Hydrogels in a historical perspective: From simple networks to smart materials. J. Control. Release 190, 254–273. http://dx.doi.org/10.1016/j.jconrel.2014.03.052, 30th Anniversary Special Issue.

Cacopardo, L., Guazzelli, N., Ahluwalia, A., 2022. Characterizing and engineering biomimetic materials for viscoelastic mechanotransduction studies. Tissue Eng. B: Rev. 28 (4), 912–925. http://dx.doi.org/10.1089/ten.teb.2021.0151, pMID: 34555953.

Chaudhuri, O., Cooper-White, J., Janmey, P.A., Mooney, D.J., Shenoy, V.B., 2020. Effects of extracellular matrix viscoelasticity on cellular behaviour. Nature 584, 535. http://dx.doi.org/10.1038/s41586-020-2612-2.

Doyle, A.D., Carvajal, N., Jin, A., Matsumoto, K., Yamada, K.M., 2015. Local 3d matrix microenvironment regulates cell migration through spatiotemporal dynamics of contractility-dependent adhesions. Nature Commun. 6, 8720. http://dx.doi.org/10.1038/ncomms9720.

Eckels, E.C., Rivas-Pardo, J.A., Valle-Orero, J., Popa, I., Fernandez, J.M., 2016. The science of stretching: Mechanical anisotropy in titin ig domains. Biophys. J. 110, 393. http://dx.doi.org/10.1016/J.BPJ.2015.11.2123a.

Farid, H., 2020. Guide to Material Calibration-Why, when and how Medical Device Designers and Analysts Should Perform Material Calibration. AVENTEC.

Fukunaga, M., Fujikawa, M., Shimizu, N., 2019. Three-dimensional finite element simulations on impact responses of gels with fractional derivative models. J. Comput. Nonlinear Dyn. 14 (revisor), http://dx.doi.org/10.1115/1.4042525.

Gagner, J.E., Kim, W., Chaikof, E.L., 2014. Designing protein-based biomaterials for medical applications. Acta Biomater. 10, 1542. http://dx.doi.org/10.1016/J.ACTBIO.2013.10.001.

García Ruíz, M.J., González, L.Y.S., 2006. Comparison of hyperelastic material models in the analysis of fabrics. Int. J. Cloth. Sci. Technol. 18 (5), 314–325. http://dx.doi.org/10.1108/09556220610685249.

Ghorbanoghli, A., Narooei, K., 2019. A new hyper-viscoelastic model for investigating rate dependent mechanical behavior of dual cross link self-healing hydrogel. Int. J. Mech. Sci. 159, 278–286. http://dx.doi.org/10.1016/j.ijmecsci.2019.06.019.

Ghoreishy, M.H.R., 2012. Determination of the parameters of the prony series in hyper-viscoelastic material models using the finite element method. Mater. Des. 35, 791–797. http://dx.doi.org/10.1016/j.matdes.2011.05.057, new Rubber Materials, Test Methods and Processes.

Heck, T., Vargas, D.A., Smeets, B., Ramon, H., van Liedekerke, P., van Oosterwyck, H., 2020. The role of actin protrusion dynamics in cell migration through a degradable viscoelastic extracellular matrix: Insights from a computational model. PLoS Comput. Biol. 16, http://dx.doi.org/10.1371/JOURNAL.PCBI.1007250.

Huerta-López, C., Alegre-Cebollada, J., 2021. Protein hydrogels: The swiss army knife for enhanced mechanical and bioactive properties of biomaterials. Nanomaterials 11, http://dx.doi.org/10.3390/nano11071656.

Huerta-Lopez, C., Clemente-Manteca, A., Velazquez-Carreras, D., Espinosa, F.M., Sanchez, J.G., Saez, P., Martinez-del Pozo, A., Garcia-Garcia, M., Martin-Colomo, S., Rodriguez-Blanco, A., Esteban-Gonzalez, R., Martin-Zamora, F.M., Gutierrez-Rus, L., Garcia, R., Roca-Cusachs, P., Elosegui-Artola, A., del Pozo, M.A., Herrero-Galan, E., Plaza, G.R., Alegre-Cebollada, J., 2022. Cell response to extracellular matrix energy dissipation outweighs rigidity sensing. BioRxiv http://dx.doi.org/10.1101/2022.11.16.516826.

Jabbari, E., 2019. Challenges for natural hydrogels in tissue engineering. Gels 5, 30. http://dx.doi.org/10.3390/gels5020030.

Javadi, M.H., Darijani, H., Niknafs, M., 2021. Constitutive modeling of visco-hyperelastic behavior of double-network hydrogels using long-term memory theory. J. Appl. Polym. Sci. 138, http://dx.doi.org/10.1002/app.49894.

Kim, T., Hwang, W., Lee, H., Kamm, R.D., 2009. Computational analysis of viscoelastic properties of crosslinked actin networks. PLoS Comput. Biol. 5 (revisor), http://dx.doi.org/10.1371/journal.pcbi.1000439.

Kim, S.R., Lee, J., Lee, E.J., Ahn, W., Lee, J.-H., 2021. Designed protein-and peptide-based hydrogels for biomedical sciences. J. Mater. Chem. B 9, 1919–1940. http://dx.doi.org/10.1039/d0tb02604b.

Kim, B., Lee, S.B., Lee, J., Cho, S., Park, H., Yeom, S., Park, S.H., 2012. A comparison among neo-hookean model, mooney-rivlin model, and ogden model for chloroprene rubber. Int. J. Precis. Eng. Manuf. 13, 759–764. http://dx.doi.org/10.1007/s12541-012-0099-y.

Krüger, M., Linke, W.A., 2011. The giant protein titin: A regulatory node that integrates myocyte signaling pathways. J. Biol. Chem. 286, 9905. http://dx.doi.org/10.1074/JBC.R110.173260.

Levental, I., Georges, P.C., Janmey, P.A., 2007. Soft biological materials and their impact on cell function. Soft Matter 3, 299–306. http://dx.doi.org/10.1039/b610522j.

Mahinroosta, M., Farsangi, Z.J., Allahverdi, A., Shakoori, Z., 2018. Hydrogels as intelligent materials: A brief review of synthesis, properties and applications. Mater. Today Chem. http://dx.doi.org/10.1016/j.mtchem.2018.02.004.

Mierke, C.T., 2022. Viscoelasticity, like forces, plays a role in mechanotransduction. Front. Cell Dev. Biol. 10, http://dx.doi.org/10.3389/fcell.2022.789841.

Narupai, B., Smith, P.T., Nelson, A., Narupai, B., Smith, P.T., Nelson, A., 2021. 4D printing of multi-stimuli responsive protein-based hydrogels for autonomous shape transformations. Adv. Funct. Mater. http://dx.doi.org/10.1002/adfm.202011012.

Palmer, J.S., Boyce, M.C., 2008. Constitutive modeling of the stress–strain behavior of f-actin filament networks. Acta Biomater. 4, 597–612. http://dx.doi.org/10.1016/J.ACTBIO.2007.12.007.

Peppas, N.A., Huang, Y., Torres-Lugo, M., Ward, J.H., Zhang, J., 2000. Physicochemical foundations and structural design of hydrogels. In: Medicine and Biology. Tech. Rep., http://dx.doi.org/10.1146/annurev.bioeng.2.1.9, Annu. Rev.Biomed..

Rassier, D.E., 2017. Sarcomere mechanics in striated muscles: From molecules to sarcomeres to cells. Am. J. Physiol. - Cell Physiol. 313, C134–C145. http://dx.doi.org/10.1152/ajpcell.00050.2017.

Ravikumar, N., Noble, C., Cramphorn, E., Taylor, Z.A., 2015. A constitutive model for ballistic gelatin at surgical strain rates. J. Mech. Behav. Biomed. Mater. 47, 87–94. http://dx.doi.org/10.1016/j.jmbbm.2015.03.011.

Romero, M.A.T., Gomez, M.D., Uribe, L.E.L., 2020. Prony series calculation for viscoelastic behavior modeling of structural adhesives from dma data. Ing. Investig. Tecnol. 21, 1–10. http://dx.doi.org/10.22201/fi.25940732e.2020.21n2.014.

Ruymbeke, E.V., Keunings, R., Stéphenne, V., Hagenaars, A., Bailly, C., 2002. Evaluation of reptation models for predicting the linear viscoelastic properties of entangled linear polymers. Macromolecules 35, 2689–2699. http://dx.doi.org/10.1021/ma011271c.

Sainz-DeMena, D., Ye, W., a, Marí., Pérez, Ángeles., José, Garcí a Aznar, M., 2022. A finite element based optimization algorithm to include diffusion into the analysis of dce-mri. Eng. Comput. 1, 3. http://dx.doi.org/10.1007/s00366-022-01667-w.

Saqlain, F., Popa, I., Fernández, J.M., Alegre-Cebollada, J., 2015. A novel strategy for utilizing voice coil servoactuators in tensile tests of low volume protein hydrogels. Macromol. Mater. Eng. 300, 369–376. http://dx.doi.org/10.1002/mame.201400271.

Shahzad, M., Kamran, A., Siddiqui, M.Z., Farhan, M., 2015. Mechanical characterization and fe modelling of a hyperelastic material. Mater. Res. 18, 918–924. http://dx.doi.org/10.1590/1516-1439.320414.

Shmilovich, K., Popa, I., 2018. Modeling protein-based hydrogels under force. Phys. Rev. Lett. 121, 168101. http://dx.doi.org/10.1103/PhysRevLett.121.168101.

Slaughter, B.V., Khurshid, S.S., Fisher, O.Z., Khademhosseini, A., Peppas, N.A., 2009. Hydrogels in regenerative medicine. Adv. Mater. 21, 3307–3329. http://dx.doi.org/10.1002/adma.200802106.

Smith, M., 2014. ABAQUS/StandArd User's Manual, Version 6.14. Dassault Systèmes Simulia Corp, United States.

Smith, D., Tanov, U., Smith, D.B., Johnson, J., Tanov, R., Komaragiri, U., 2010. Calibration of Nonlinear Viscoelastic Materials in Abaqus using the Adaptive Quasi-Linear Viscoelastic Model. Tech. Rep., Dassault Systems SIMULIA.

Stowers, R.S., Shcherbina, A., Israeli, J., Gruber, J.J., Chang, J., Nam, S., Rabiee, A., Teruel, M.N., Snyder, M.P., Kundaje, A., Chaudhuri, O., 2019. Matrix stiffness induces a tumorigenic phenotype in mammary epithelium through changes in chromatin accessibility. Nat. Biomed. Eng. 3, 1009–1019. http://dx.doi.org/10.1038/s41551-019-0420-5.

Valero, C., Amaveda, H., Mora, M., García-Aznar, J.M., 2018. Combined experimental and computational characterization of crosslinked collagen-based hydrogels. PLoS One http://dx.doi.org/10.1371/journal.pone.0195820.

Wozniak, M.A., Chen, C.S., 2009. Mechanotransduction in development: A growing role for contractility. Nat. Rev. Mol. Cell Biol. 10, 34–43. http://dx.doi.org/10.1038/nrm2592.

Wu, J., Li, P., Dong, C., Jiang, H., Xue, B., Gao, X., Qin, M., Wang, W., Chen, B., Cao, Y., 2018. Rationally designed synthetic protein hydrogels with predictable mechanical properties. Nature Commun. http://dx.doi.org/10.1038/s41467-018-02917-6.

Yang, C., Tibbitt, M.W., Basta, L., Anseth, K.S., 2014. Mechanical memory and dosing influence stem cell fate. Nature Mater. http://dx.doi.org/10.1038/NMAT3889.

You, J.-O., Auguste, D.T., 2010. Properties of solids; electrical resistivity of pure metals. Int. J. Microcirc. Clin. Exp. 26, 6283. http://dx.doi.org/10.1021/la100294p.